RSC Advances

PAPER

View Article Online
View Journal | View Issue

Check for updates

Cite this: *RSC Adv.*, 2026, **16**, 285

Towards the selectivity and energetics of anti-Bredt olefins – a density functional theory approach

Pritam Chakraborty,† Jannat Alam,† Bibitha Poulose, Shyama Ramakrishnan and Padmesh Anjukandi *

Received 26th November 2025
Accepted 16th December 2025

DOI: 10.1039/d5ra09135g

rsc.li/rsc-advances

Anti-Bredt olefins (ABOs) are scarce owing to the double bond at bridgehead carbon in small bicyclic systems and also due to their effective geometrical constraints that hinder the p-orbital overlap. However, of late, people have been interested in synthesizing ABOs so as to harness their strain energy. Invention of novel stabilizing techniques and advancement in the synthesis procedures has led to a growing interest in these molecules. Recently, it was identified that a certain chemical precursor can be used to generate an ABO as an intermediate. The unique geometries and electronic properties of these could offer valuable alternatives synthetic routes in both medicinal chemistry and catalysis. In this study, we utilize Density Functional Theory (DFT) to comprehensively examine the energetics, reaction mechanism, and structural implications of ABO generation. Exhaustive energy profiling allows us to evaluate both the thermodynamic stability and kinetic barriers, revealing details about reaction feasibility. To summarize, this study offers a fundamental understanding of the molecular-level factors that influence the energetics, formation, and stability of ABO.

Open Access Article. Published on 02 January 2026. Downloaded on 1/22/2026 10:41:35 AM.
This article is licensed under a Creative Commons Attribution-NonCommercial 3.0 Unported Licence.

1 Introduction

Olefins are highly reactive molecules that play a central role in synthetic chemistry, with applications ranging from olefin metathesis[1–4] and polymerization[5,6] to the preparation of functionalized derivatives used in pharmaceuticals, agrochemicals, and other organic syntheses.[7] A special class of these compounds, known as anti-Bredt olefins (ABOs), contain a double bond at the bridgehead position (see Fig. 1). Due to the inherent strain in their structure, ABOs once synthesized can serve as valuable and useful unique intermediates in synthetic chemistry.

In 1900s, Julius Bredt was studying bicyclic compounds such as camphane and pinane and observed that these structures were unable to form carbon–carbon double bonds at the bridgehead positions.[8–12] In his experiments, Bredt attempted the elimination of hydrogen bromide from bicyclic bromocamphoric acid anhydride but found that the expected double bond did not form. Similarly, the corresponding unsaturated dicarboxylic acid failed to cyclize into an anhydride.[8,11] Based on these findings, Bredt concluded in 1924 that the formation of a carbon–carbon double bond at the bridgehead carbon atoms of a bridged bicyclic system is not possible which is now known as "Bredt's rule". It is mainly applicable to bicyclo[*m.n.o*] alkane systems. In a broader sense, in any polycyclic system having bridges, the carbon–carbon and carbon-nitrogen double bond at the bridge heads are not acceptable.[9]

The double bond in the bridgeheads will be twisted, thus distorting the geometry, which will lead to ring strain, but if the number of atoms in the ring system is large, then a double bond can be formed in the bridgehead positions.[8] Bredt's rule is also applied to determine if the reaction and the desired product will be formed or not. Natural products with bridgehead double bonds do exist[13] and with the help of olefin strain energy, it is predicted that some of the natural products with bridgehead double bonds are isolable.[9,14] In a recent study[15] Wang *et al.* have utilized Bredt's Rule to make better fluorescent dyes for super-resolution fluorescence microscopy.

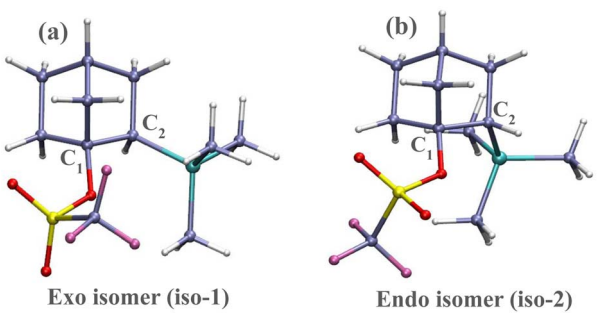

Fig. 1 Starting bicyclic compounds. (a) 2-*exo*-trimethylsilyl-1-trifluoromethanesulfonyl-bicyclo[2.2.1]heptane. and (b) 2-*endo*-trimethylsilyl-1-trifluoromethanesulfonyl-bicyclo[2.2.1]heptane.

Department of Chemistry, Indian Institute of Technology, Palakkad 678557, Kerala, India. E-mail: padmesh@iitpkd.ac.in

† These authors contributed equally to the work.

© 2026 The Author(s). Published by the Royal Society of Chemistry

Open Access Article. Published on 02 January 2026. Downloaded on 1/22/2026 10:41:35 AM. This article is licensed under a Creative Commons Attribution-NonCommercial 3.0 Unported Licence.

Thus, ABOs are generally strained and unstable when their ring systems are small. ABOs contain alkenes with remarkably distorted geometries that feature unsymmetrical twisting and pyramidalization of each terminus.[16] This type of highly strained molecule can be used in the synthesis of natural products, structurally complex products with the help of cycloadditions, in the synthesis of drugs and in bioorthogonal chemistry.[16–18] ABOs with twisted double bonds can also undergo 2 + 2 cycloaddition reactions.[19] Anti-Bredt's bridgehead nitrogen compounds are used in the synthesis of polymers because of their inherent strain with the help of ring-opening polymerization.[20] ABO precursors can be used in the synthesis of drugs like taxol. So in spite of the existence of Bredt's rule, many researchers have tried synthesizing ABOs, like Marshall,[21] Wiseman,[22,23] and Keese[24] with the help of elimination reactions, and Platz,[25] and Eguchi[26] have taken advantage of carbene rearrangement[27] to generate ABOs.[16] A silicon analogue of the smallest anti-Bredt olefin *i.e.*, bicyclo[1.1.0]but-1(2)-ene, is synthesized and stabilized by base.[28] Among the recent studies[29,30] on anti-Bredt olefins, one report highlights that direct geometry optimization of the β-halo carbanion precursor gives ABO.[30]

Recently, McDermott *et al.*[16] were successful in synthesizing two precursors, e*xo* isomer (iso-1) and *endo* isomer (iso-2) (see Fig. 1) where they could capture the corresponding ABO from iso-1 by syn elimination, which was trapped using anthracene as a trapping agent *via* cycloaddition reaction. Iso-2 remained inanimate towards the reaction and the energetics and mechanism of this ABO formation are yet to be completely understood. Considering the growing interest in ABO across various areas of chemistry, elucidating its formation pathway is of considerable significance. In particular, they also observed that iso-2 could not induce any ABO product, as the TMS group and the OTf group were not syn periplanar as discussed, raising key questions. Why does one isomer lead to ABO formation while the other does not? How does geometry influence this difference? In this work, we try and address these questions using Density Functional Theory (DFT) calculations to provide explicit mechanistic and energetic insights.

2 Methodology

The computational studies were carried out using the ORCA[31] software package. The BP86 (ref. 32) functional, together with the SVP basis set and D3BJ[33] dispersion correction, was employed for calculations. One-dimensional Potential Energy Surface (PES) scan and Nudge Elastic Band (NEB) were performed to obtain a preliminary understanding of the energetics of the reaction pathway connecting the reactant and product. The maxima and minima identified from these PES scans were then optimized to determine whether they correspond to transition states or true minima. Subsequently, a two-dimensional PES scan was conducted on the pentacoordinated siliconate complex by systematically varying the C_1–OTf distance and the C_2–Si distance. Finally, Natural Bond Orbital (NBO) analysis was performed to investigate charge distribution and the nature of the atomic orbitals involved in the olefin formation. All the reactant and product geometries were optimized and verified to possess no imaginary frequencies. The transition state was optimized and characterized by the presence of a single imaginary frequency, corresponding to the expected vibrational mode of the reaction pathway. In some cases, additional imaginary frequencies were observed in the reactant, product, and transition state structures. These modes were identified as arising from methyl group rotations and, therefore, were considered non-essential and neglected in the analysis.

$$k = \frac{\kappa k_B T}{hC^\circ} \exp\left(-\frac{\Delta G^\ddagger}{RT}\right) \quad (1)$$

The forward and backward rate constants were calculated using the Eyring equation[34] (1). The Eyring equation relates reaction rate constants to temperature through transition state theory, enabling calculation of forward and backward rate constants from activation parameters. Here, k = rate constant, κ = transmission coefficient, k_B = Boltzmann constant, h = Planck's constant, C° = standard concentration, $\Delta G^\ddagger$ = Gibbs free energy of activation, R = gas constant, T = temperature (K).

3 Results and discussion

To gain qualitative insight into the reaction energetics, we first performed a one-dimensional potential energy surface scan to examine the approach of the F^- ion toward the silicon atom of the TMS group (Fig. 2(a)). This analysis reveals the formation of a stable pentacoordinated siliconate complex (PCC) for both isomers, and the process is essentially barrierless. Starting from this stable PCC, we subsequently increased the C_1–OTf distance in both isomers (Fig. 2(b)), while Fig. 2(c) illustrates the elongation of the C_2–Si bond in iso-2. To get deeper insight into why iso-1 forms ABO whereas iso-2 does not, we steered an elaborate DFT investigation towards the energetics along the respective reaction pathways (see Fig. 3). For iso-1&2, the reactions were initiated by the approach of the fluoride ion (F^-) towards the Si of the [$Si(CH_3)_3$] group. It is clearly observed that in both the cases, F^- initially gets engaged in to dipole–dipole interactions with the methyl substituent, and further, they are stabilized by the formation of a pentacoordinated siliconate complex (**B** and **D**, respectively, in Fig. 3), which is maintained by a stable trigonal bipyramidal geometry, and they are stabilized by a free energy difference of ~16.5 ± 1 kcal mol^{-1}(see Fig. 2(a) for a detailed potential energy scan and Fig. S15 for the geometrical features of these intermediates. The energy scan shows that the formation of the pentacoordinated siliconate complex is mostly a down-the-hill process). Further towards the formation of ABO in the case of iso-1, the reaction pathway (blue curve in Fig. 3) was additionally explored. The pentacoordinated siliconate complex (**B**) eliminates both the leaving groups (OTf^- followed by $Si(CH_3)_3F$), proceeding *via* a transition state (TS-1) to yield the ABO product (**C**) with a free energy barrier ($\Delta G^\ddagger_{iso\text{-}1}$) of ~6 kcal mol^{-1}. In the case of iso-2, it follows a similar but significantly more energy-demanding pathway (brown curve), with an activation energy barrier ($\Delta G^\ddagger_{iso\text{-}2}$) of ~34 kcal mol^{-1}. The ABO (**F**) formed from iso-2 is found to be higher in energy compared to

 © 2026 The Author(s). Published by the Royal Society of Chemistry

Open Access Article. Published on 02 January 2026. Downloaded on 1/22/2026 10:41:35 AM.
This article is licensed under a Creative Commons Attribution-NonCommercial 3.0 Unported Licence.

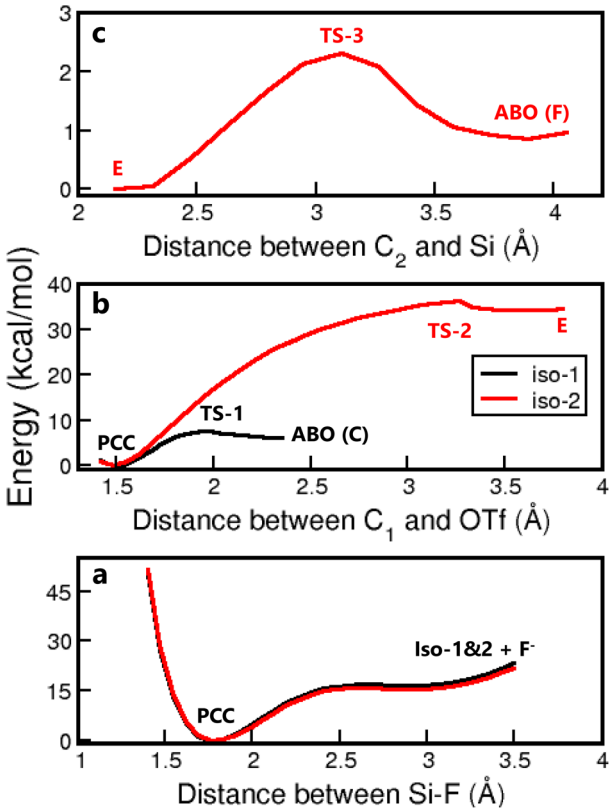

Fig. 2 Potential energy surface scan (a) depicting the approach of the fluoride ion toward the silicon atom of the TMS group, leading to the formation of a pentacoordinated siliconate complex (PCC) for iso-1 (black) and iso-2 (red). (b) Illustrating the dissociation of the OTf group from the stable pentacoordinated siliconate complex. (c) Illustrating the dissociation of the TMSF group for iso-2.

ABO (**C**) from iso-1, which could be associated with the geometric instabilities of the ABO structures (see Table S2 in SI) obtained from both. Yet another major difference in the ABO formation between the iso-1 and iso-2 is that in the former case, the leaving groups leave more or less in a concerted fashion after the pentacoordinated siliconate complex formation whereas in the latter, it requires the leaving of the OTf^- completely and then the leaving of the $Si(CH_3)_3F$ group to facilitate the formation of the ABO. To understand the kinetics of the ABO formation from iso-1&2, the forward and backward rate constants of the important steps (as represented along the arrows in Fig. 3) along both the pathways were calculated using the eqn (1). In the case of iso-1, both the forward and backward rate constants for the **B** to **C** transformation are very high, indicating an equilibrium constant of approximately 3 between the ABO product (**C**) and the pentacoordinated siliconate complex (**B**) (see SI Section 7 for further details). This scenario implies that **C** has a fair chance to revert back (rates are of comparable order) to the pentacoordinated siliconate complex (**B**). Thus the ABO (**C**) could be a transient species, which is quite consistent with experimental observations[16] as they were unable to capture (**C**) directly. In contrast, for iso-2, the transition state (TS-2) clearly shows that the OTf^- group has left, while the C_2–Si bond is still intact. The bond length analysis reveals the C_2–Si and C_1–C_2 distance of semi-ABO(E) as 2.21 Å and 1.43 Å, respectively, indicating that the C_2–Si bond is already weak at this separation and that the C_1–C_2 bond is no longer a proper single bond (see Fig. S2 of SI). However, the forward rate constant for the **D** to **E** transformation in iso-2 is much smaller, which implies that the formation of the product is kinetically disfavored. Even if the product forms, the high backward rate suggests that it will rapidly revert to the pentacoordinated siliconate complex (**D**).

The two different isomers of the bicyclic compound (iso-1 & iso-2) exhibit distinct energetics for ABO formation; iso-1 progresses through a low activation energy pathway, whereas iso-2 requires a significantly higher activation energy. To explain this disparity, we revisited Bredt's rule, which affirms that the presence of a double bond at a bridgehead carbon is generally unfavorable due to geometric constraints that hinder effective p-orbital overlap. This in turn suggests that the unfavorable geometry of the systems should directly influence the p-orbital overlap at the bridgehead position of the bicyclic systems. Essentially, the effectiveness of the p-orbital overlap depends on the key factors: their symmetry and the energy alignment. In order to substantiate the understanding of the atomic orbital interactions at the bridgehead carbon, we performed Natural Bond Orbital (NBO) analysis[35,36] along C_1–OTf bond length, and the information on the atomic orbitals in the form of Natural Atomic Orbitals (NAOs)[37,38] was extracted along the reaction coordinate in the pentacoordinated siliconate complex (**B**). The results of these analyses are summarized in Fig. 4. A C_1–OTf bond length of around ~1.45 Å represents a stable pentacoordinated siliconate complex, while its extension to ~1.79 Å signifies the departure of OTf^- and the onset of ABO formation. The orbital energies overlap where one has a proper bond between C_1 and C_2. Thus Fig. 4(a) exhibits an overlap at ~1.48 Å of C_1–OTf bond length, where it denotes a C_1 and C_2 σ bond in the pentacoordinated siliconate complex (**B**). Further along the variation of the C_1–OTf bond length, at ~1.79 Å, the OTf^- has completely detached, indicating the formation of the product (**C**) with the separation of the $Si(CH_3)_3F$ group, forming a C_1 and C_2 double bond with the help of $2p_x$ (C_1)–$2p_x$ (C_2) energy overlap (see Fig. 4(b) for details). In contrast, p_y–p_y and p_z–p_z overlaps are not feasible in iso-1 due to significant energy mismatches between the respective orbitals. For iso-2, none of the orbital combinations with the same symmetry (p_x–p_x, p_y–p_y, p_z–p_z) exhibit effective overlap, as all the cases exhibit substantial energy differences between the interacting orbitals, except that of the C_1 and C_2 σ bond (see SI Fig. S14). This lack of orbital energy mismatch in iso-2 results in poor π-bond formation capability at the bridgehead position, consistent with its high activation barrier for ABO formation. We also examined all the possible combinations of p-orbital overlaps between C_1 and C_2 (see Tables S5 and S6 of SI). Thus, the NAO analysis very clearly depicts the formation of the bridgehead double bond in iso-1 and the incapability of iso-2 owing to the orbital energy and symmetry mismatch.

Although we have a rigorous understanding of the energetics of ABO formation from iso-1 and iso-2, as well as how the

© 2026 The Author(s). Published by the Royal Society of Chemistry

Open Access Article. Published on 02 January 2026. Downloaded on 1/22/2026 10:41:35 AM.
This article is licensed under a Creative Commons Attribution-NonCommercial 3.0 Unported Licence.

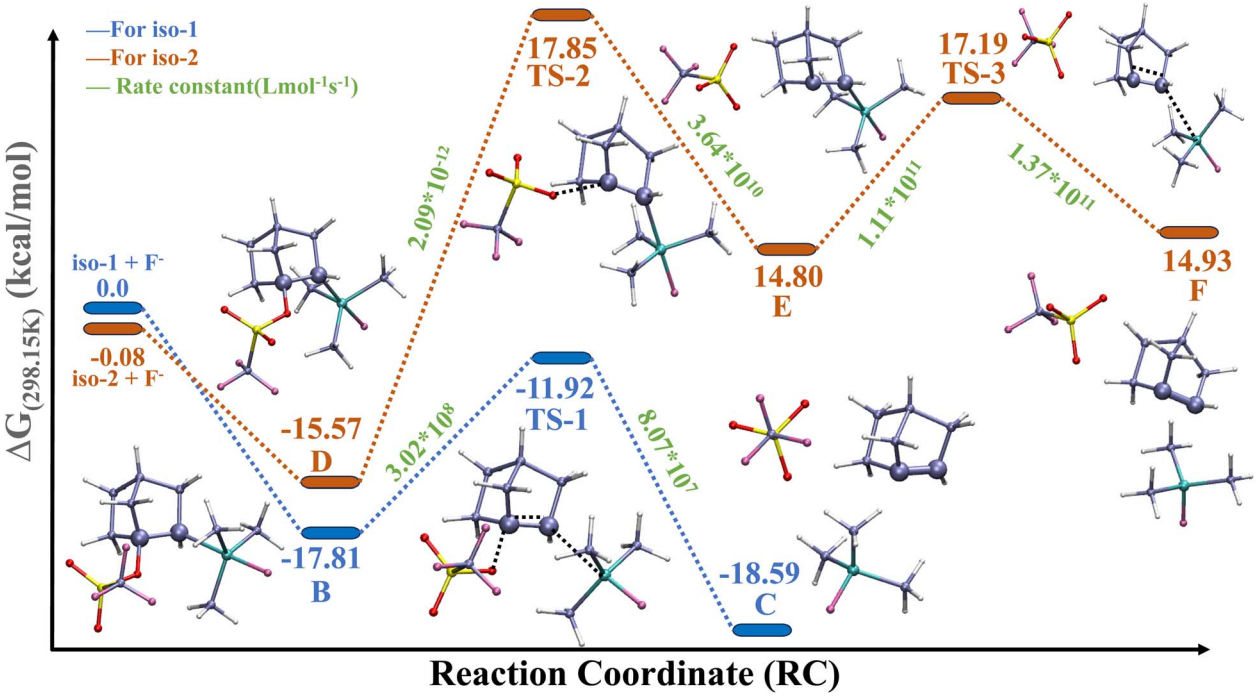

Fig. 3 Energy profile for the formation of ABO for both the precursor iso-1 and iso-2. When fluoride ion is coming, the ABO is formed through the formation of a stable pentacoordinated siliconate complex. The blue profile corresponds to iso-1, and the brown energy profile corresponds to iso-2. The free energies are calculated with respect to iso-1. The rate constants in relevant cases for the forward and backward reactions are mentioned along the paths.

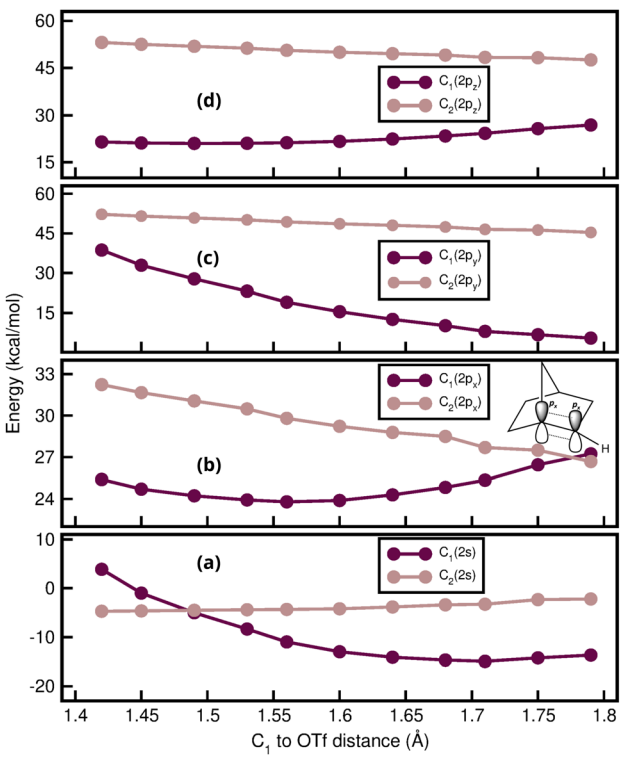

Fig. 4 Calculation of the symmetry and energy differences between the valence shell atomic orbitals of the bridgehead carbon atoms (C_1 and C_2) in iso-1 was performed using Natural Atomic Orbital (NAO) analysis: (a) for 2s orbital, (b) for $2p_x$ orbital, (c) for $2p_y$ orbital and (d) for $2p_z$ orbital.

geometry of iso-2 hinders p-orbital overlap between C_1 and C_2, the major concern remains regarding the mechanism of ABO formation in iso-1. Thus, to gain deeper insight into the mechanism of ABO formation from iso-1, we performed a two-dimensional potential energy surface (see Fig. 5(a)) scan along the reaction pathway with C_1–OTf and C_2–Si bond distances as reaction coordinates. Fig. 2(a) reveals that formation of the pentacoordinated siliconate complex (PCC) from both isomers proceeds *via* an almost barrierless process. Once the stable PCC forms, it can follow three distinct elimination mechanisms resembling E1, E1cb, and E2 pathways to generate the anti-Bredt olefin. In the E1-like mechanism, departure of the –OTf group (a good leaving group) first produces a tertiary carbocation at the bridgehead carbon (C_1), followed by elimination of the $SiMe_3F$ (TMSF) moiety. The E1cb-like mechanism involves initial elimination of the stable $SiMe_3F$ (TMSF) group to yield a secondary carbanion adjacent to the bridgehead carbon (C_2), with subsequent loss of –OTf. Finally, the E2-like mechanism entails nearly simultaneous expulsion of both –OTf and $SiMe_3F$ (TMSF) groups in a concerted manner, directly affording the anti-Bredt olefin (see Section 4 of SI for details). In Fig. 5(a) the yellow line highlights the minimum energy path (MEP) along the 2D surface. The formation of the pentacoordinated siliconate complex already weakens the C_2–Si bond by elongating it to ~2.1 Å, which is quite visible in the surface. Further the release of the OTf^- (bonded at ~1.45 Å of C_1–OTf) group initially affects the C_2–Si bond length (which denotes the release of $Si(CH_3)_3F$ group) only slightly. But the moment C_1–OTf length reaches

© 2026 The Author(s). Published by the Royal Society of Chemistry

Open Access Article. Published on 02 January 2026. Downloaded on 1/22/2026 10:41:35 AM.
This article is licensed under a Creative Commons Attribution-NonCommercial 3.0 Unported Licence.

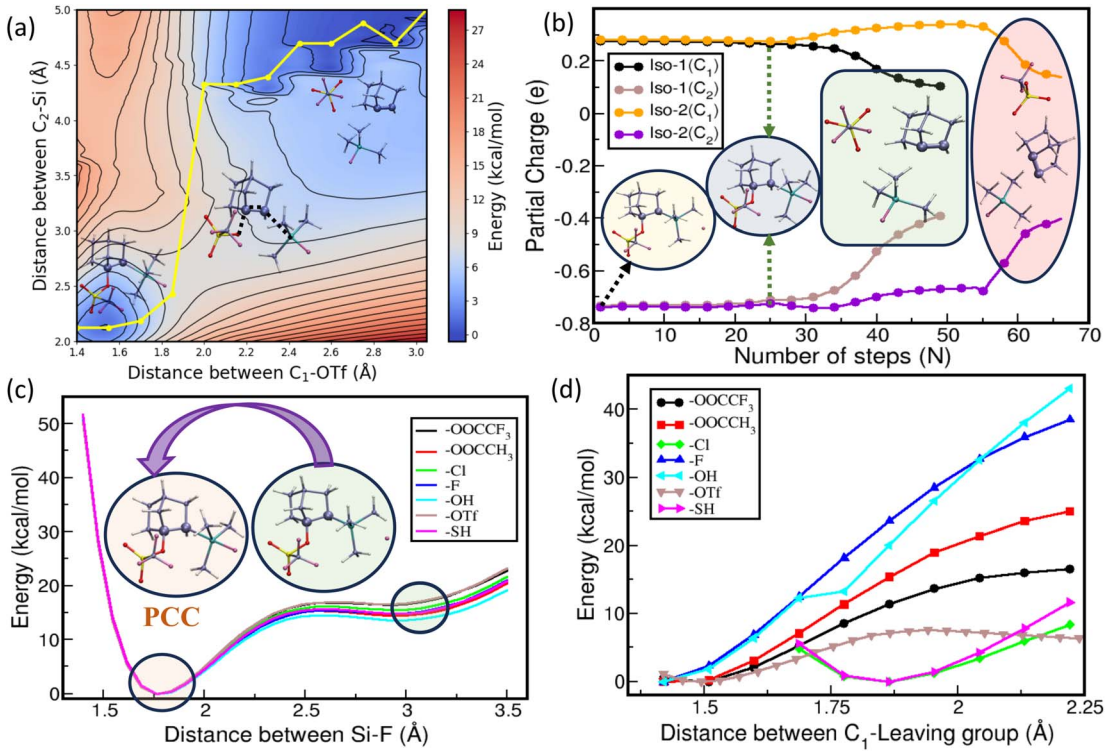

Fig. 5 (a) Two-dimensional potential energy surface of iso-1 by taking the stable pentacoordinated siliconate complex as the starting point: *x*-axis is the C–OTf bond distance (d_1) and *y*-axis is the C–Si bond distance (d_2). (b) Charge analysis of both isomers was conducted during the approach of the F^- ion toward the Si atom. For both isomers, the first 25 steps correspond to pentacoordinated siliconate complex (PCC) formation, followed by steps 26–49 for iso-1 and 26–66 for iso-2 during ABO formation. 1D-dimensional potential energy surface scan: (c) when the fluoride is coming and making the stable pentacoordinated siliconate complex (PCC), (d) taking the pentacoordinated siliconate complex (PCC), the leaving of the leaving group and TMSF, and the formation of the ABO.

~1.8 Å, $Si(CH_3)_3F$ group also gets detached, as is pointed out by the sharp rise of the yellow MEP. This suggests that the breaking of the C_1–OTf bond initiates the process, subsequently promoting the dissociation of the C_2–Si bond. The energy for this process is found to be of the order of ~12 kcal mol^{-1}, suggesting that this could be a fast reaction and mostly constitute to a nearly syn elimination, mostly a concerted process (third mechanism).

Together, we also performed an NBO charge analysis on C_1 and C_2 for both isomers (Fig. 5(b)) along the reaction pathway. Here, the *X*-axis (number of steps) represents a combined 1D scan coordinates of the Si–F bond distance (1–25 steps) and the C_1–OTf bond distance (26–49 steps for iso-1 and 26–66 for iso-2) (see Tables S3 and S4 in SI for further details), starting from the initial precursor (iso-1 and iso-2 separately) and ending at the product. The *Y*-axis corresponds to the partial charges obtained from the NBO analysis. Thus the initial 25 points along the horizontal axis correspond to the formation of the Si–F bond to form the pentacoordinated siliconate complex. Further, from 26 to 49 (iso-1) steps corresponds to the cleavage of the C_1–OTf bond. In the case of iso-1 (brown and black curves), the partial charges on C_1 and C_2 remain nearly constant up to step 25 and gradually tend to decrease on C_1 and increase on C_2 as the C_2–Si bond of TMS and the C_1–OTf bond begin to dissociate, marking the formation of the C_1=C_2 double bond in the ABO product. In contrast, for iso-2 (violet and orange curve), no significant variation in the partial charges is observed until the final product initiation at the 56th step and finally forming the product (66th step), suggesting that even if the C_1–OTf bond is dissociated, $Si(CH_3)_3F$ group does not leave until it is forced to do so (see Table S4 in SI). The role of the leaving group OTf^- being very crucial for the formation of the ABO, we also examined the effect of different leaving groups on the formation of ABO in iso-1 by systematically substituting the poor ($-SH^-$, $-OH^-$, $-F^-$) to moderate (CH_3COO^-), and good (CF_3COO^-, Cl^-) leaving groups (see Fig. 5(c) and (d)). Fig. 5(c) depicts the reaction corresponding to the approach of F^- towards the TMS group, where the pentacoordinated siliconate complex is formed. The energy profiles suggest that irrespective of the leaving group, the profiles remain nearly identical, suggesting a biased process towards the pentacoordinated siliconate complex, which is not affected by the nature of the leaving group. But however, in the second case (Fig. 5(d)), corresponding to the scan between C_1 and the leaving group where the ABO is formed, the energy barriers varied significantly depending on the leaving group. While all the others were favoring a downhill process towards the reactant (pentacoordinated siliconate complex), OTf^- exhibited the lowest energy barrier two-state process (brown curve) and is hence identified as the most energetically favorable leaving group,

Open Access Article. Published on 02 January 2026. Downloaded on 1/22/2026 10:41:35 AM. This article is licensed under a Creative Commons Attribution-NonCommercial 3.0 Unported Licence.

consistent with experimental observations. Thus, the energy profile diagram (Fig. 3) reveals that the formation of ABO from iso-1 is energetically favorable, whereas in the case of iso-2 it is a high energy demanding process.

4 Conclusions

In summary, we demonstrate here the formation of the ABOs from two precursor isomer molecules, iso-1 and iso-2. The calculations show that the activation energy for forming the ABO from the exo isomer (iso-1) is more feasible than from the endo isomer (iso-2). Further, the energetics of the NAOs of iso-1 and iso-2 clearly demonstrate how the subtle difference in the geometry separates the energy level of the p_x orbitals in the endo form, thus not allowing the olefin formation. The 2-D energy surface and the partial charge analysis elaborately define the mechanism of the formation of the ABO in iso-1, confirming a possible syn-elimination of the leaving groups to form the product. Finally, regarding the role of the leaving group, it is clear from our simulations that the whole process of the ABO formation in iso-1 is guided by the dissociation of the OTf^-, subsequently of the $Si(CH_3)_3F$ group. Thus assessing the role of different leaving groups at C_1 position, it is evident that the formation of the pentacoordinated siliconate complex(PCC) is not affected by the nature of the leaving group and towards the formation of the ABO, OTf^- at C_1 position seems to be the best possible bet, which is in line with the existing experimental finding.

Author contributions

P. A. conceptualized and administered the work. P. C., J. A., B. P. and S. R. conducted the modeling and simulations of the systems. P. A., P. C. and J. A. contributed towards the result analysis and preparation of the draft manuscript.

Conflicts of interest

The authors declare no competing interest.

Data availability

The data supporting this article have been included as part of the supplementary information (SI). Supplementary information: detailed description of the methodology and computational details, description of the physical parameters for iso-1 and iso-2, detailed descriptions regarding the potential energy scans performed, mechanistic details for the formation of anti-Bredt olefin, discussion of the nudge elastic band calculation and its results, details on the rate constant (k) calculation using the Eyrings equation, description of the relation between rate constant (k) and equilibrium constant (K), discussion on the Natural Bond Orbital (NBO) partial charge and Natural Atomic Orbital (NAO) analysis performed, structural details and features of the pentacoordinated siliconate complex (PCC) of iso-1, details on the partial charge analysis of pentacoordinated complexes by NBO and coordinate details for all the optimised structures. See DOI: https://doi.org/10.1039/d5ra09135g.

Acknowledgements

The authors thank IIT Palakkad for providing them with CHANDRA and MADHAVA supercomputing facility and also thank IIT Palakkad (Grant Number: 2024-238-CHY-PAA-ERG-SP) for the generous funding and support.

References

1 S. Rogalski and C. Pietraszuk, *Molecules*, 2023, **28**(4), 1680.
2 P. Żak and C. Pietraszuk, *Beilstein J. Org. Chem.*, 2019, **15**, 310–332.
3 R. L. Pederson, I. M. Fellows, T. A. Ung, H. Ishihara and S. P. Hajela, *Adv. Synth. Catal.*, 2002, **344**, 728–735.
4 D. Zárate-Saldaña, B. Landeros-Rivera, J. A. Cruz-Morales and S. Gutiérrez, *J. Organomet. Chem.*, 2020, **913**, 121206.
5 K. J. Ivin, J. J. Rooney, C. D. Stewart, M. L. Green and R. Mahtab, *J. Chem. Soc. Chem. Commun.*, 1978, 604–606.
6 Y. Imanishi and N. Naga, *Prog. Polym. Sci.*, 2001, **26**, 1147–1198.
7 L. McDermott, Z. G. Walters, A. M. Clark and N. K. Garg, *Nat. Synth.*, 2025, **4**, 421–431.
8 G. Köbrich, *Angew Chem. Int. Ed. Engl.*, 1973, **12**, 464–473.
9 F. S. Fawcett, *Chem. Rev.*, 1950, **47**, 219–274.
10 G. Buchanan, *Chem. Soc. Rev.*, 1974, **3**, 41–63.
11 J. Bredt, *Justus Liebigs Ann. Chem.*, 1924, **437**, 1–13.
12 J. Bredt, J. Houben and P. Levy, *Ber. Dtsch. Chem. Ges.*, 1902, **35**, 1286–1292.
13 J. Y. Mak, R. H. Pouwer and C. M. Williams, *Angew. Chem., Int. Ed.*, 2014, **53**, 13664–13688.
14 E. H. Krenske and C. M. Williams, *Angew. Chem., Int. Ed.*, 2015, **54**, 10608–10612.
15 F. Brøndsted and L. G. Wang, *Nat. Methods*, 2025, **22**, 1137–1139.
16 L. McDermott, Z. G. Walters, S. A. French, A. M. Clark, J. Ding, A. V. Kelleghan, K. Houk and N. K. Garg, *Science*, 2024, **386**, eadq3519.
17 C. M. Gampe and E. M. Carreira, *Angew. Chem., Int. Ed.*, 2012, **51**, 3766–3778.
18 F. Xie, H. Jiang, X. Jia, J. Zhang, Z. Zhu, J. Du and Y. Tang, *Org. Lett.*, 2022, **24**, 5304–5308.
19 R. V. Viesser, C. P. Donald, J. A. May and J. I. Wu, *Org. Lett.*, 2024, **26**, 3778–3783.
20 H. Hall Jr and A. El-Shekeil, *Chem. Rev.*, 1983, **83**, 549–555.
21 J. A. Marshall and H. Faubl, *J. Am. Chem. Soc.*, 1967, **89**, 5965–5966.
22 J. R. Wiseman, *J. Am. Chem. Soc.*, 1967, **89**, 5966–5968.
23 J. R. Wiseman and J. A. Chong, *J. Am. Chem. Soc.*, 1969, **91**, 7775–7777.
24 R. Keese and E.-P. Krebs, *Angew Chem. Int. Ed. Engl.*, 1971, **10**, 262–263.
25 N. Chen, M. Jones Jr, W. R. White and M. S. Platz, *J. Am. Chem. Soc.*, 1991, **113**, 4981–4992.

© 2026 The Author(s). Published by the Royal Society of Chemistry

Open Access Article. Published on 02 January 2026. Downloaded on 1/22/2026 10:41:35 AM.
This article is licensed under a Creative Commons Attribution-NonCommercial 3.0 Unported Licence.

26 M. Ohno, M. Itoh, M. Umeda, R. Furuta, K. Kondo and S. Eguchi, *J. Am. Chem. Soc.*, 1996, **118**, 7075–7082.
27 C. M. Geise and C. M. Hadad, *J. Am. Chem. Soc.*, 2000, **122**, 5861–5865.
28 T. Iwamoto, N. Akasaka and S. Ishida, *Nat. Commun.*, 2014, **5**, 5353.
29 J. Zhang, X. Wang and T. Xu, *Nat. Commun.*, 2021, **12**, 3022.
30 G. W. Breton and J. V. Ridlehoover, *Organics*, 2024, **5**, 205–218.
31 F. Neese, *Wiley Interdiscip. Rev.: Comput. Mol. Sci.*, 2012, **2**, 73–78.
32 J. P. Perdew, K. Burke and M. Ernzerhof, *Phys. Rev. Lett.*, 1996, **77**, 3865.
33 S. Grimme, S. Ehrlich and L. Goerigk, *J. Comput. Chem.*, 2011, **32**, 1456–1465.
34 H. Eyring, *J. Chem. Phys.*, 1935, **3**, 107–115.
35 I. Sabeeh Hasan, A. A. Majhool, M. H. Sami, M. Adil and S. S. S. A. Azziz, *Chem. Rev. Lett.*, 2023, **6**, 297–307.
36 E. D. Glendening and F. Weinhold, *Chem. Phys. Lett.*, 2018, **711**, 23–26.
37 A. E. Reed and F. Weinhold, *J. Chem. Phys.*, 1983, **78**, 4066–4073.
38 A. E. Reed, R. B. Weinstock and F. Weinhold, *J. Chem. Phys.*, 1985, **83**, 735–746.

© 2026 The Author(s). Published by the Royal Society of Chemistry